

## Analyte preconcentration in nanofluidic channels with nonuniform zeta potential

A. Eden,<sup>1,\*</sup> C. McCallum,<sup>1</sup> B. D. Storey,<sup>2</sup> S. Pennathur,<sup>1</sup> and C. D. Meinhart<sup>1,†</sup>

<sup>1</sup>*Department of Mechanical Engineering, University of California Santa Barbara, Santa Barbara, California 93101, USA*

<sup>2</sup>*Olin College of Engineering, Olin College, Needham, Massachusetts 02492, USA*

(Received 13 April 2017; published 21 December 2017)

It is well known that charged analytes in the presence of nonuniform electric fields concentrate at locations where the relevant driving forces balance, and a wide range of ionic stacking and focusing methods are commonly employed to leverage these physical mechanisms in order to improve signal levels in biosensing applications. In particular, nanofluidic channels with spatially varying conductivity distributions have been shown to provide increased preconcentration of charged analytes due to the existence of a finite electric double layer (EDL), in which electrostatic attraction and repulsion from charged surfaces produce nonuniform transverse ion distributions. In this work, we use numerical simulations to show that one can achieve greater levels of sample accumulation by using field-effect control via wall-embedded electrodes to tailor the surface potential heterogeneity in a nanochannel with overlapped EDLs. In addition to previously demonstrated stacking and focusing mechanisms, we find that the coupling between two-dimensional ion distributions and the axial electric field under overlapped EDL conditions can generate an ion concentration polarization interface in the middle of the channel. Under an applied electric field, this interface can be used to concentrate sample ions between two stationary regions of different surface potential and charge density. Our numerical model uses the Poisson-Nernst-Planck system of equations coupled with the Stokes equation to demonstrate the phenomenon, and we discuss in detail the driving forces behind the predicted sample enhancement. The numerical velocity and salt concentration profiles exhibit good agreement with analytical results from a simplified one-dimensional area-averaged model for several limiting cases, and we show predicted amplification ratios of up to  $10^5$ .

DOI: [10.1103/PhysRevFluids.2.124203](https://doi.org/10.1103/PhysRevFluids.2.124203)

### I. INTRODUCTION

A constantly evolving understanding of natural biological processes coupled with advances in micro- and nanoscale fabrication technologies has recently spurred the development of myriad novel devices for bioassays, protein and DNA separation and amplification, and other lab-on-chip processes [1–7]. The small scale of these devices introduces many obstacles that must be overcome through engineering prowess, however, and a primary concern in the field remains the necessity for sample analyte preconcentration in bioanalytical micro- and nanofluidic devices [2,8]. Innovative focusing techniques utilizing electrokinetic phenomena such as field-amplified sample stacking (FASS) [8–11], ion concentration polarization [12–17], isotachopheresis [18], isoelectric focusing [19], concentration gradient focusing [20], and many others have been introduced to address and resolve this prevalent issue. In many such cases, anionic analyte focusing is achieved by exploiting the competition between electroosmotic flow (EOF) and electrophoresis in order to drive the anionic species to a location where the upstream electrophoretic velocity balances the downstream bulk

---

\*a\_eden@engineering.ucsb.edu

†meinhart@engineering.ucsb.edu

electroosmotic fluid flow [10,14,16]. These enriched ions can then be interrogated, separated, or otherwise manipulated for further downstream processing once the level of sample molecules reaches the threshold limit for the desired application, allowing for increased sensitivity of bioanalytical devices [12,15].

In traditional field-amplified sample stacking methods, electric field gradients are used to drive analyte ions to an interface between a background solution and an injected plug of lower conductivity fluid [8]. This effect occurs regardless of the electric double layer (EDL) thickness and can thus be achieved in microscale channels and/or with higher electrolyte concentrations in nanochannels. Sustarich *et al.* [10] discovered that in nanochannels, greater FASS enhancement ratios can be obtained due to flow focusing and electrostatic repulsion of sample ions towards the channel center by finite-sized but nonoverlapping EDLs. These FASS techniques produce short-lived enhancement, however, as they require a propagating plug which is prone to diffusion and dispersion due to pressure gradients induced by nonuniform EOF [9]. In the regime of overlapped EDLs, other approaches such as concentration polarization (CP) leverage the charge-selective nature of EDL structures by generating stationary or propagating “shock” zones of ion accumulation or depletion near permselective microchannel-nanochannel junctions, as first visualized by Pu *et al.* [12] and later described in detail by Mani *et al.* [14] and Zangle *et al.* [15]. They found that these CP phenomena are primarily governed by the background electrolyte (BGE) concentration, the analyte mobility, the channel height, the induced surface charge that establishes the EDL structure, and the applied electric field strength. All of these factors determine the nature and extent of the observed concentration polarization, and therefore the subsequent analyte preconcentration capabilities of CP-based methods.

Researchers have also previously investigated the effects of nonuniform EOF due to spatially varying surface properties realized through field-effect control and/or various surface treatments. Schasfoort *et al.* [21] first presented a device they designated a “flow field-effect transistor” which allowed for local zeta potential and electroosmotic flow control through field-effect modulation via a gate electrode near the channel wall. Herr *et al.* [22] later developed a simple one-dimensional (1D) model to represent nonuniform EOF in a capillary with a step change in zeta potential due to surface adsorption of an EOF-suppressing polymer. Fu *et al.* [23] investigated a similar configuration of heterogeneous zeta potential in more detail by accounting for local ion distributions and electroosmotic advection using a Nernst-Planck model. More complex models have since been generalized to represent micro- and nanofluidic systems with arbitrary nonuniform surface charge and/or variable heights [14,16,24]. Applications ranging from integrated fluid field-effect transistors to nanofluidic diodes have also emerged following fundamental discoveries reported by researchers such as Karnik *et al.* [25] and Daiguji *et al.* [26], respectively; as a result of this research and other similar works [1,27–33], nanofluidic channels with nonuniform surface potential have been shown to exhibit tremendous promise when it comes to controlling the behavior of bulk fluid and individual ions on-demand. Moreover, Jin and Aluru [32] showed that in addition to exhibiting FET properties, nanochannels with wall-embedded electrodes used to tailor the surface charge and potential can be leveraged for variable analyte stacking by tuning the applied gate voltage. To our knowledge, however, no studies to date have investigated in-depth the preconcentration capabilities of nanochannels with nonuniform surface properties achieved through field-effect control.

The remainder of this paper is organized as follows. In Sec. II, we present the underlying governing equations for ion transport in the nanofluidic system, and we describe in detail our two-dimensional (2D) numerical model along with the simulated boundary conditions. The preconcentration simulation results are presented in Sec. III, in which we discuss the causes and limitations of the predicted sample enhancement. We reveal that the mechanisms which lead to sample accumulation are effectively the same as the driving forces behind FASS and CP, as field-effect surface charge modulation can induce axial gradients in the ionic conductivity distribution and generate concentration polarization interfaces between distinct regions of the channel due to large area-averaged EDL gradients. These combined effects are shown to only occur in nanochannels with

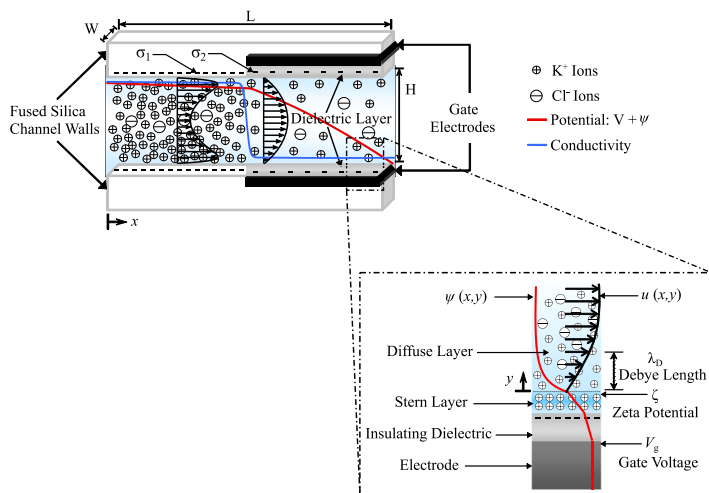


FIG. 1. Diagram of the described nanofluidic device with embedded electrodes in the top and bottom channel walls, showing example ion distributions in a channel with modified surface charge and potential (top center), as well as the EDL potential and velocity profiles near an embedded electrode (bottom right).

sufficiently large EDLs relative to the channel height, and in channels with nonuniform zeta potential. Our results predict achievable sample enhancement ratios which exceed those from traditional FASS by more than two orders of magnitude [10,11]. Finally, we conclude by summarizing the main points of our findings in Sec. IV.

## II. THEORETICAL AND NUMERICAL FRAMEWORK

### A. Nanofluidic system

The system we are modeling consists of a nanofluidic channel with embedded, addressable electrodes along half of the channel length (see Fig. 1). These gate electrodes, which are isolated from the fluid within the channel by a thin dielectric layer, allow for field-effect modulation of the local surface charge density and electric potential at the fluid-solid interface in this region of the channel. The nanochannel connects two reservoirs which are significantly larger than the channel and are filled with a solution of background electrolyte ions. In nanofluidic systems such as this, high geometric aspect ratios generally result in channels with very small height-to-width ratios ( $H/W \ll 1$ ), and therefore a depth-averaged 2D analysis is a reasonable approximation of the transport conditions.

### B. Governing equations and 2D numerical model

The foundation for ion transport within the channel is the Poisson-Nernst-Planck system of equations, which accounts for the local ion distributions arising from electrostatic interactions with the charge-regulated channel walls. These equations are coupled with the Navier-Stokes equations to account for the advective transport of ions through the channel due to electroosmotic flow from an applied electric field [23,24]. Since the nanofluidic channel is long and thin, it is convenient to separate the local electrostatic potential of the fluid into a potential  $V$  associated with the applied electric field, which varies in the axial direction inside the channel, and an intrinsic EDL potential  $\psi$  which can vary in both the axial and transverse directions for nonuniform EOF cases. Separating the EDL and applied potentials in this manner facilitates comparison between our numerical simulations and the 1D area-averaged verification model presented in the Supplemental Material [34] and is

similar to the approach found in previous works which assume that the EDLs are in equilibrium in the transverse direction [14,24,32] but can vary in the axial direction due to effects such as CP.

We use Poisson's equation to relate the electrostatic potential distribution throughout the fluid to the spatial free charge density of ions in solution,

$$-\varepsilon_0\varepsilon_f\nabla^2(V + \psi) = \rho_E, \quad (1)$$

where  $\varepsilon_0$  is the permittivity of free space,  $\varepsilon_f$  is the dielectric constant of the electrolyte solution (assumed to be a constant  $\varepsilon_f = 80.1$ ),  $\rho_E$  is the local volumetric charge density,  $V$  is the potential associated with an applied electric field, and  $\psi$  is the local EDL potential. The charge density  $\rho_E$  effectively represents the net free charge present due to a local imbalance of cations and anions in solution and can be expressed as  $\rho_E = F \sum_{i=1}^m z_i c_i$ , where  $F$  is Faraday's constant,  $z_i$  is the ion valence of species  $i$ ,  $c_i$  is the molar concentration, and  $m$  is the number of species in solution. Following previous works, we assume that the concentration of sample ions is much lower than the BGE ion concentrations, such that the sample has a negligible influence on the charge density [10,15]. The local potential  $V + \psi$  is specified to be equal to an applied potential at the top boundary of the inlet reservoir and grounded at the top boundary of the outlet reservoir, while the EDL potential  $\psi$  is locally equal to the zeta potential  $\zeta$  at the channel and reservoir walls. As reported by Stein *et al.* [35], the resulting surface charge can be related to the potential gradient at the wall using the relation  $\sigma_s = \varepsilon_0\varepsilon_f\mathbf{n} \cdot \nabla\psi$ , where  $\mathbf{n}$  is the outward surface normal unit vector.

The concentrations of background electrolyte ions and ionic sample species within the channel and reservoirs are determined using mass conservation. Extending Fick's macroscale diffusion law to account for electroosmotic advection as well as transverse and axial electromigration of ionic species in a dilute BGE solution, we define the mass conservation equation for species  $i$  as

$$\frac{\partial c_i}{\partial t} = -\nabla \cdot [\mathbf{u}c_i - D_i\nabla c_i - \mu_i z_i F c_i \nabla(V + \psi)]. \quad (2)$$

Here  $D_i$  is the ion diffusivity,  $z_i$  is the ion valence,  $\mu_i$  is the mobility,  $F$  is Faraday's constant, and  $\mathbf{u}$  is the fluid velocity. The convective flux  $\mathbf{u}c_i$  accounts for ion transport due to electroosmotic advection, while the diffusive flux  $-D_i\nabla c_i$  represents ion diffusion in the presence of a local concentration gradient. The combined electromigration flux  $-\mu_i z_i F c_i \nabla(V + \psi)$  accounts for axial and transverse migration from variations in the EDL potential  $\psi$ , as well as the additional axial electromigration once an applied potential  $V$  is introduced across the channel. Therefore, the total flux of species  $i$  is given by  $\mathbf{N}_i = \mathbf{u}c_i - D_i\nabla c_i - \mu_i z_i F c_i \nabla(V + \psi)$ . As a consequence of Eq. (2), the net current density  $\mathbf{J} = F \sum_{i=1}^m z_i \mathbf{N}_i$  associated with BGE ion transport is divergence free at steady state.

We consider a dilute binary background electrolyte solution where  $c_+$  is the cation concentration,  $c_-$  is the anion concentration, and  $c_s$  is the sample species concentration. The ion mobilities are calculated using the Nernst-Einstein mobility equation  $\mu_i = \frac{D_i}{RT}$ , where  $R$  is the universal gas constant and  $T$  is the solution temperature, assumed to be fixed at 20 °C. The boundary conditions associated with Eq. (2) include bulk concentration Dirichlet conditions  $c_i = c_{i,\infty}$  and  $c_s = c_0$  for the BGE and sample species, respectively, at the reservoir inlet and outlet. A zero normal species flux condition  $\mathbf{n} \cdot \mathbf{N}_i = 0$  is enforced at the solid walls of the nanochannel and reservoirs, which are assumed to be impermeable.

Finally, the inherently low Reynolds number associated with nanofluidic flows allows us to use the incompressible form of the Stokes' equation and the continuity equation to describe the conservation of momentum within the nanochannel for a fluid experiencing a Coulombic body force due to a nonzero free charge distribution,

$$0 = \eta\nabla^2\mathbf{u} - \nabla P - \rho_E\nabla(V + \psi); \quad \nabla \cdot \mathbf{u} = 0, \quad (3)$$

where  $P$  is the pressure within the fluid and  $\eta$  is the dynamic viscosity of the fluid. The fluid gauge pressure relative to atmosphere is specified to be zero at the inlet and outlet of the reservoirs, while a no slip condition  $\mathbf{u} = 0$  is enforced at the nanochannel and reservoir walls.

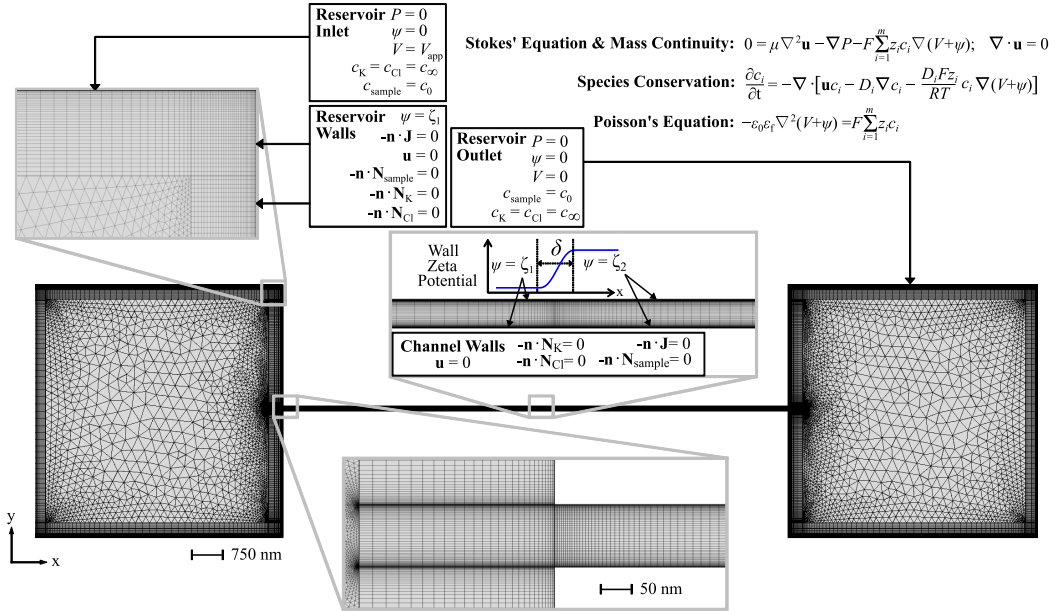


FIG. 2. COMSOL mesh and boundary conditions for the 2D numerical model.

We use COMSOL v5.1 to numerically simulate the highly coupled, nonlinear system of Eqs. (1)–(3). Since we assume a very dilute sample concentration, we first solve for the final steady state transport conditions in the BGE and then use these results to separately solve for the temporal and steady state concentrations of the sample species. Our model also assumes a fixed surface potential at the walls and constant ion mobilities, both of which are often used in analytical and numerical models but are not always found to be true in practice [35,36]. We included fluid reservoirs located at the channel inlet and outlet in order to allow for a more realistic treatment of the boundary conditions at the free surface of the fluid (see Fig. 2), as well as to account for any concentration polarization effects at the channel inlet and outlet. The zeta potential along the channel was modeled as a smoothed, continuous step function which transitions over  $\delta = 5 \text{ nm}$ . The unmodified wall zeta potentials are chosen to be representative of previously reported values for various pH and electrolyte concentrations [37], while the gate voltages required to produce the desired modified zeta potentials are estimated for future experimental verification using the theory of Hughes *et al.* [38] for nonoverlapped EDLs and the theory of Yeh *et al.* [39] for overlapped EDLs.

In order to verify that our 2D numerical simulations yield reasonable results for the BGE conditions, we compare the results to a simplified 1D area-averaged model which captures most, but not all, of the important physics (see Supplemental Material [34]). The most significant shortcoming of this 1D model is that it neglects diffusion and concentration polarization effects arising from the application of an external field across a permselective nanochannel with overlapped EDLs. However, Mani *et al.* [14] showed that these CP effects are negligible when the accumulation and depletion regions near a nanochannel inlet and outlet do not extend beyond a diffuse region near the interface (referred to as nonpropagating CP) and the Peclet number  $Pe = UL/D$  is sufficiently large. We therefore restrict the use of our 1D verification model to (1) nonoverlapped EDL cases and (2) high Pe overlapped EDL cases without appreciable CP propagation. Including these effects would make a simple 1D model intractable, so we instead use the 1D area-averaged model to verify our numerical simulations for these simpler limiting cases (see Supplemental Material [34]) and then investigate more complex conditions using the 2D numerical results presented in Sec. III.

### III. RESULTS

#### A. Possible enhancement mechanisms within the nanochannel

For the current nanochannel configuration in which an embedded electrode controls the zeta potential in the right half of the channel, there are three possible mechanisms which can contribute to sample accumulation inside the channel itself: stacking, focusing, and focusing at a midchannel CP interface. Both cationic and anionic preconcentration can also be achieved near the channel inlet or outlet via stacking and/or focusing by leveraging CP effects at stationary or propagating “shocks” of ion accumulation and depletion at different interfaces within the reservoirs; Zangle *et al.* [15] comprehensively reviewed the various experimentally observed and theoretically predicted stacking and focusing mechanisms at these locations, so we direct our focus to investigating stacking and focusing within the domain of a nanochannel with nonuniform zeta potential.

Mani *et al.* [14] described a useful characteristic analysis which utilizes a dimensionless mobility defined as the ratio of the migration speed of species  $i$  to the bulk electroosmotic velocity,  $v_i^* = \frac{U_i^{\text{eph}}}{U_{\text{bulk}}}$ , in order to predict the direction of analyte information propagation in different regions of the system (and therefore whether stacking or focusing occurs) through simple scaling arguments. We adopt this approach by scaling the analytical EOF profile for region 2 of a nonuniform channel to obtain  $v_{2,i}^* = -\frac{v_i|z_i|F\eta E_2}{\varepsilon_0\varepsilon_f(3E_1\zeta_1-4E_2\zeta_2)}$  (see Supplemental Material [34] for the nonuniform EOF profile). Note that our definition differs from the conventional definition  $v_i^* = \frac{v_i z_i F \eta}{\varepsilon_0 \varepsilon_f \zeta}$  of Mani *et al.* [14], but reduces to the same result for the limiting case of  $E_1 = E_2$  and  $\zeta_1 = \zeta_2$ . This distinction arises because our nonuniform channel leads to different induced pressure gradients and electric fields in the two regions, such that the dimensionless mobility varies within the channel. The bulk flow velocity must have the same scale in both regions by continuity, so similarly for region 1 we have  $v_{1,i}^* = -\frac{v_i|z_i|F\eta E_1}{\varepsilon_0\varepsilon_f(3E_1\zeta_1-4E_2\zeta_2)}$ .

For an anionic species, a dimensionless mobility  $v_{2,i}^* > 1$  describes an analyte for which the upstream electrophoretic velocity in region 2 exceeds the downstream bulk flow speed, leading to net upstream analyte transport in that region. Conversely, a dimensionless mobility of  $v_{2,i}^* < 1$  predicts that the same analyte will travel downstream in region 2 because the bulk flow speed exceeds the electrophoretic velocity. In such a case, the anionic sample will not be able to enter the channel from the outlet reservoir and thus no preconcentration is possible inside the channel [15,16]. The electric field in each region can be roughly estimated to calculate the dimensionless mobility by approximating the EDLs as thin [10,14] to obtain  $E_2/E_1 \sim \sigma_1/\sigma_2$ , and then by using the Grahame equation to obtain  $E_2/E_1 \sim \sinh(\frac{Fz\zeta_1}{RT})/\sinh(\frac{Fz\zeta_2}{RT})$  [41] for symmetric electrolytes.

The first possible enhancement mechanism within the nanochannel, stacking, occurs when the background flow conditions predict average anionic sample velocities in each region which are not equal but are still in the same direction, i.e., when  $v_{2,i}^* > v_{1,i}^* > 1$ . This transport velocity difference effectively leads to a “traffic jam” of ions because sample ions are predicted to move upstream faster in region 2 than in region 1. This is the effect observed in Fig. 3(a) in which the ion concentration in one of the two regions must increase in order to balance the flux of ions moving through each region at steady state. This is also the same underlying mechanism found in classical field-amplified sample stacking, as described by Burgi and Chien [8]. In the current configuration, however, FASS-like stacking can be achieved in a stationary manner without the need for a propagating injected plug solution. Note that this type of midchannel stacking would be achieved using higher concentration BGE solutions in which the EDLs do not overlap and is therefore not a direct consequence of CP. For overlapped EDLs, concentration polarization effects would manifest and the third mechanism would dominate the predicted enhancement.

The second mechanism, focusing under nonoverlapped EDL conditions, occurs when the transport velocity of an anionic species is upstream in region 2 but downstream in region 1, i.e., when  $v_{2,i}^* > 1 > v_{1,i}^* > 0$ . In such situations, the sample is predicted to be driven from both sides to a single location of maximum accumulation near the zeta potential transition, as shown in Fig. 3(b). This type of focusing occurs in our channel when the electrophoretic velocity exceeds the bulk flow

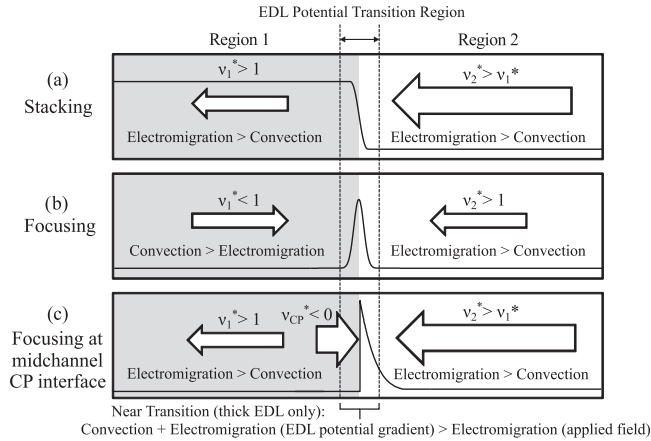


FIG. 3. Diagram of the three possible enhancement mechanisms: stacking, focusing, and focusing at a midchannel CP interface. Curves depict sample concentration profiles, while arrows show the direction and relative magnitude of the net sample ion transport velocity in each region before steady state is reached.

speed in region 2 but not in region 1, a condition which can be satisfied by specific combinations of zeta potentials, electric fields, and velocity profiles in each region. Whether stacking or focusing occurs in the channel depends on the dimensionless mobility and is therefore highly dependent on sample mobility and valence. In general, samples of lower mobility will tend to become focused because the decreased mobility lowers  $v_{1,i}^*$  sufficiently that the opposing convection can exceed electromigration and change the direction of the analyte transport in region 1. This mechanism was discussed at length by Sustarich *et al.* [10], who showed that finite but nonoverlapping EDLs can enhance the level of observed focusing.

The third possible mechanism is also considered focusing but occurs only for thick EDL cases. This effect arises from the axial potential gradient between regions of different area-averaged EDL potential and has previously proven to be useful in concentrating charged samples at microchannel-nanochannel interfaces [13–16]. This effect differs from the focusing described above in that the dimensionless mobility in region 1 does not necessarily have to drop below unity. Rather, in this case there exists a small diffusion-limited transition region at the CP interface in which the dimensionless mobility actually changes sign across the interface because the coupling between the area averaged EDL potential gradient and the applied electric field can effectively reverse the net electric field direction in this location (see Sec. III B for further explanation). A dimensionless mobility greater than unity in both region 1 and region 2 would subsequently lead to a strongly polarized interface with depletion on the left side and accumulation on the right side (see Fig. 3). Since the first two mechanisms have been thoroughly investigated in Refs. [9] and [10], respectively, we chose to limit the scope of the current study to investigating a regime of overlapped EDLs with nonuniform zeta potentials in which the third mechanism is the principal cause of analyte accumulation.

The enhancement from sample stacking can easily be estimated by the ratio of predicted sample fluxes in each region [8,15], while the nonoverlapped EDL focusing mechanism requires some incorporation of diffusion in order to properly model. Focusing capabilities for such conditions are still largely determined by the ion fluxes in the fully developed areas far from the zeta potential transition, however, and analytical theory can still be used to estimate the level of sample enhancement from this type of focusing by including axial diffusion [10]. In contrast, the third mechanism is dominated by a very localized CP effect near the transition and thus cannot be quantitatively predicted using a simple 1D model; a more complete numerical treatment is required when the nonuniform EDLs are overlapped in order to fully capture all of the driving forces which contribute to this type of CP-based focusing within the channel.

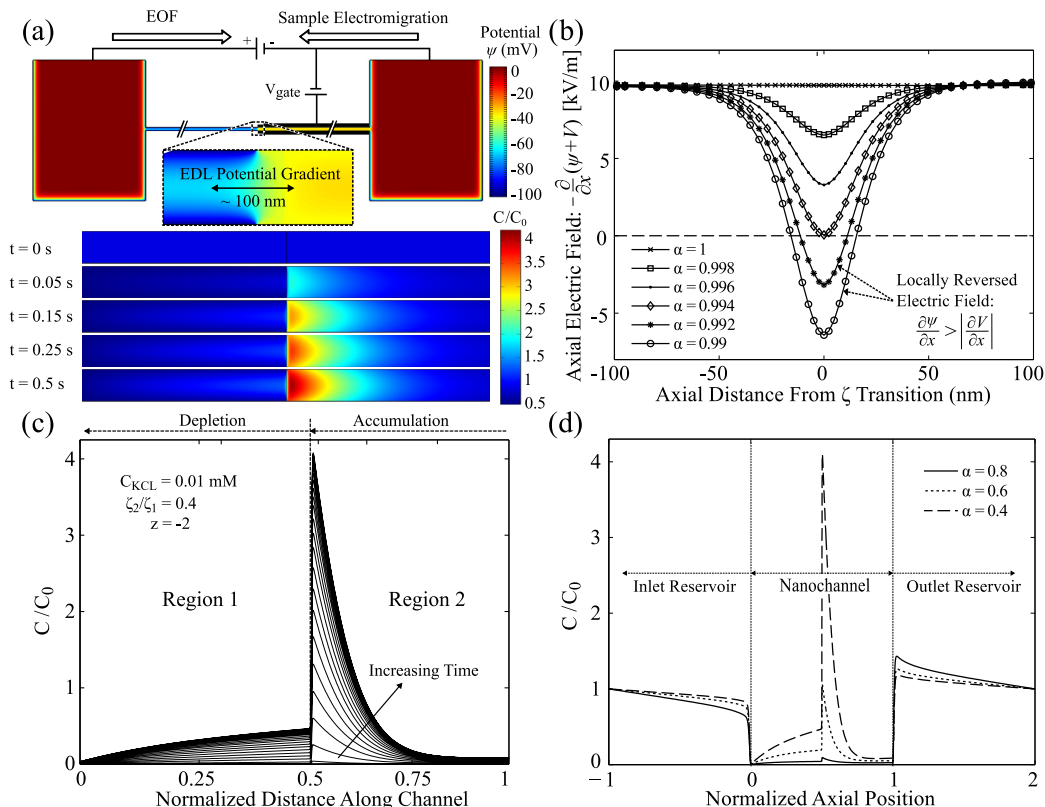


FIG. 4. (a) EDL potential near the midchannel CP interface along with the transient evolution of a 2D sample concentration profile in the channel, (b) the net electric field along the centerline near the midchannel CP interface, (c) the temporal sample profile along the channel center, and (d) the steady state sample concentration along the centerline for varying zeta potential ratio  $\alpha = \zeta_2/\zeta_1$ . The axial EDL potential gradient is visible in (a), and its effect on the sample transport is evident from the reversal of the net electric field in (b) as well as the CP-induced analyte focusing in (c) and (d). The zeta potential ratio and BGE concentration for these simulations of a 20  $\mu\text{m}$  long, 100 nm tall channel were fixed at  $\alpha = 0.4$  and  $C_{KCl} = 0.01$  mM, respectively, unless otherwise specified.

### B. Analyte focusing using nonuniform, overlapped EDLs: 2D simulation results

We demonstrate how an anionic sample analyte with valence  $z = -2$  and diffusivity  $D_s = 0.5 \times 10^{-9} \text{ m}^2 \text{ s}^{-1}$  accumulates near an interface where a smooth step change in zeta potential occurs (see Fig. 4). Specifically, Fig. 4(a) depicts the temporal evolution of a 2D sample concentration profile within a 20  $\mu\text{m}$  long, 100 nm tall channel. We fixed the sample concentration at 1 pM at the top of the BGE inlet and outlet reservoirs for these simulations, such that the sample ions migrate left through the channel under the influence of the applied field. The unmodified zeta potential was fixed at  $-100$  mV, while the modified zeta potential was  $-40$  mV and the nominal electric field strength was 10 kV/m.

The intrinsic EDL potential  $\psi$  along the centerline remains nonzero throughout the channel due to the overlapped EDLs, leading to an axial gradient in the area-averaged EDL potential near the zeta potential transition. Since the axial electric field  $E_x = -\left(\frac{\partial V}{\partial x} + \frac{\partial \psi}{\partial x}\right)$  is a coupled combination of the applied electric field and the axial EDL potential gradient, its direction can change sign locally at certain locations depending on the sign and magnitude of  $\frac{\partial \psi}{\partial x}$  relative to  $\frac{\partial V}{\partial x}$ . Figure 4(a) shows how this gradient in the net electric field enhances sample accumulation in the middle of the channel

by effectively creating an electrophoretic trapping region at this CP interface. The presence of a similar electrostatic potential gradient at the channel outlet suggests that an anionic analyte will not be able to enter the channel unless diffusion and electromigration from the applied field can drive ions past this interface. The magnitude of the zeta potential  $\zeta_2$  near the outlet is therefore critical in determining whether sample ions are able to enter the channel, as suggested by the form of the dimensionless mobility  $v_{2,i}^*$ . By controlling  $\zeta_2$  with embedded electrodes in the top and bottom walls, this area-averaged potential gradient can be lowered sufficiently that the combined effect of diffusion and electromigration from an external electric field overcomes the CP at the channel outlet, allowing for sample transport into the channel.

A simple analysis suggests that net the electric field should locally change direction at a CP interface when the local EDL potential gradient exceeds the local electric field from the applied potential, or  $\frac{\partial\psi}{\partial x} > |\frac{\partial V}{\partial x}|$ . By estimating this EDL potential gradient as the change in zeta potential over some transition length scale assumed to be on the order of the Debye screening length, it is predicted that an approximate difference in zeta potentials exceeding just 1 mV leads to  $\frac{|\zeta_2 - \zeta_1|}{\lambda_D} > \frac{V_{app}}{L}$ , and thus  $E_x < 0$ , for a 10 kV/m applied field in a 0.01 mM KCl solution ( $\lambda_D \approx 100$  nm). Our simulation results in Fig. 4(b) show that this local electric field reversal indeed occurs when  $\zeta_1$  and  $\zeta_2$  differ by more than about 0.6 mV. Although this effect occurs for very small variations in  $\alpha = \frac{\zeta_2}{\zeta_1}$ , we do not see appreciable focusing of ions within the channel when  $\zeta_2$  is sufficiently negative, such as in the  $\alpha = 0.8$  case in Fig. 4(d), because CP at the outlet almost entirely excludes all sample ions from entering the channel.

To understand the temporal distribution of sample ions throughout the channel in Figs. 4(a) and 4(c), we further examine the role of the net electric field and corresponding sample fluxes. The electric field in region 2 is higher than that in region 1 due to the lower density of BGE ions (fewer ions are needed to screen the smaller zeta potential), and thus any sample ions that are able to enter the channel are driven towards region 1 with a large electrophoretic velocity. Sample ions near the region 2–region 1 transition are slowed when approaching the EDL potential gradient at the CP interface, which is large enough to reverse the direction of the net electric field in this case. In this diffusion-limited transition zone, the electrophoretic flux and convective flux are both positive (to the right) and only the diffusive flux is negative (to the left). The diffusive flux is initially relatively small, so the overall imbalance of fluxes causes the sample to rapidly become focused near the location where the net electric field changes direction. After the sample sufficiently accumulates, the concentration gradient which controls the diffusive flux becomes large enough to drive sample ions past this stationary CP “shock” and into region 1. Once the sample enters region 1, electromigration and a strong diffusive flux drive the ions further upstream into the BGE inlet reservoir, easily overcoming the opposing convective flux and leading to further localized sample depletion as ions are rapidly accelerated out of the channel. Eventually the diffusive, electromigrative, and convective fluxes start to balance and the system approaches equilibrium. The spatiotemporal centerline sample concentration converges to a constant profile as the system reaches steady state, as shown in Fig. 4(c).

### C. Maximum enhancement and limiting behavior

The maximum achievable sample concentration enhancement for overlapped EDL conditions is governed by CP phenomena, and is therefore primarily a function of EDL thickness, zeta potential ratio, sample charge and mobility, and the applied electric field. Figure 5 shows thick EDL sample focusing within a 50 nm tall channel, demonstrating the maximum concentration enhancement achievable as these control parameters are varied. Significant accumulation occurs near the zeta potential transition for our simulated conditions only when the nonuniformities in potential and ion distributions throughout the channel are noticeable; that is, when the zeta potential magnitudes in regions 1 and 2 differ sufficiently and the EDLs overlap to create a midchannel CP interface. A moderate level of stacking or focusing can potentially be observed in the regime of nonoverlapped EDLs for certain sample mobilities and BGE conditions, but our results in Fig. 5(a) indicate that the

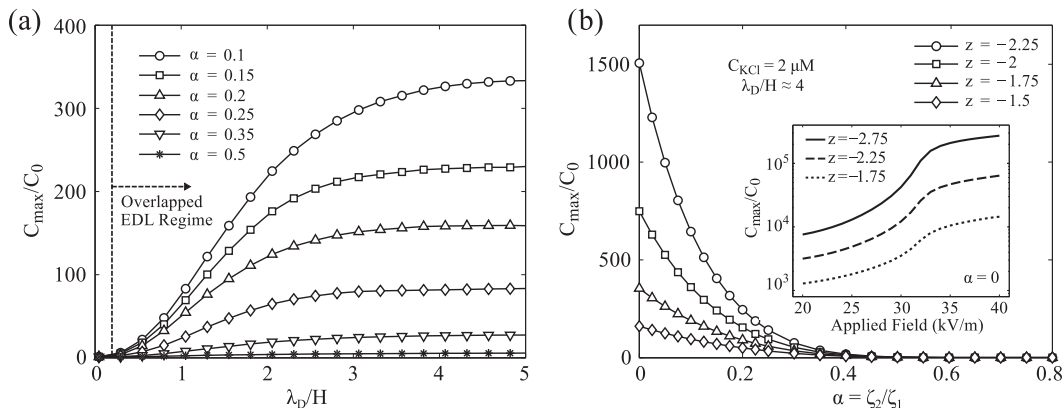


FIG. 5. Sample enhancement is shown in (a) for varying zeta potential ratios and EDL thicknesses for a fixed 50 nm channel height and 10 kV/m applied field and in (b) for varying zeta potential, sample charge, and applied field. The zeta potential in region 1 was fixed at  $-100$  mV for these simulations, while the sample valence for (a) was fixed at  $z = -2$ . The corresponding KCl concentrations in (a) range from 50 mM to 1.5  $\mu$ M. The inset plot in (b) shows maximum concentration enhancement for  $\alpha = 0$  as the applied electric field is increased to 40 kV/m.

simulated sample with a mobility of  $3.9 \times 10^{-8} \text{ m}^2 \text{ V}^{-1} \text{ s}^{-1}$  (roughly representative of fluorescein) is not predicted to appreciably accumulate anywhere in the channel when the EDLs are not overlapped.

More interesting effects manifest as we explore sample enhancement in the limit of thick EDLs. Figure 5(a) demonstrates that the level of sample enhancement increases as the EDLs become much thicker relative to the channel height and the magnitude of  $\zeta_2$  decreases, i.e., as the midchannel CP interface becomes more prominent and the CP interface at the outlet starts to disappear. Fig. 5(b) shows that the extent of CP at the outlet is limited enough to allow a large number of sample ions to enter the channel and accumulate near the zeta potential transition only when  $\alpha < 0.5$  for these conditions. Specifically, the results show that the sample is locally enhanced by greater than an order of magnitude in the middle of the channel when  $\alpha$  drops below approximately 0.45 for  $\lambda_D/H \approx 4$  if  $\zeta_1$  is fixed at  $-100$  mV.

As the concentration is decreased below 1 mM, the enhancement in Fig. 5(a) first increases dramatically and then starts to saturate as the system reaches a state in which there are such few ions to screen the charged walls that the potential and ion distributions are essentially the same at the centerline as they are at the wall. This limiting behavior leads to an area-averaged EDL potential gradient that approaches a constant value as the concentration is decreased beyond a critical threshold for a given channel height and fixed zeta potentials. As this potential gradient governs the CP which leads to sample focusing, the enhancement ultimately reaches a plateau for very low BGE concentrations if all other simulation parameters are held fixed. Figure 5(b) shows that because highly charged sample ions experience stronger interactions with field gradients near the transition, ions of sufficiently high valence can effectively be concentrated by up to five orders of magnitude by increasing the applied electric field strength. The curves for  $z = -1.75$  are representative of fluorescein ions, and the predicted 6200-fold enhancement of this sample at 32 kV/m roughly constitutes a factor of 45 increase compared to injection-based FASS results with the same sample and applied field [10].

#### D. Assumptions and limitations

As with any simulation, it is important to understand the assumptions and limitations of our numerical model. First, we note again that  $\zeta_1$  is fixed at  $-100$  mV for these idealized simulations, so practical variations in  $\zeta_2$  would only be achievable by modulating the gate voltage for a fixed solution

$pH$ . While the choice of the zeta potential transition length  $\delta = 5$  nm in our numerical model is somewhat arbitrary, our results show that the choice of  $\delta$  does not appreciably affect the results for a range of  $2 \text{ nm} < \delta < 200 \text{ nm}$  with a background concentration of  $C_{\text{KCl}} = 0.01 \text{ mM}$ . This can be explained through the observation that the centerline potential profile in the diffusion-limited transition region, and thus the axial EDL potential gradient, is relatively insensitive to  $\delta$  unless it is varied by several orders of magnitude and is well outside the predicted range of values (see the Supplemental Material [34]); preliminary simulations of the 2D governing Eqs. (1)–(3) with a discontinuous surface charge boundary condition indicate that the surface potential transition length ranges from approximately 2 to 150 nm depending on  $\alpha$ , while a previously published numerical simulation of embedded electrodes suggests that the transition is on the order of a few nanometers [3]. Therefore, we fixed the transition length at  $\delta = 5$  nm for the purposes of this study.

A background electrolyte concentration of less than  $1 \mu\text{M}$  is impractical to simulate in the limit of small  $\alpha$ , as the sample ions will begin to accumulate sufficiently that the maximum concentration would be within an order of magnitude of the BGE concentration. In such a case, the analyte would noticeably contribute to the charge density and corresponding EDL potential distributions near the midchannel CP interface (recall that this contribution is neglected in the current model). However, practically achieving ionic concentrations below  $1 \mu\text{M}$  is difficult since ions in pure water are generally in the nM concentration range. Furthermore, these low concentration conditions would introduce complications in the experimental characterization and validation of the devices; the conductivity of electrolyte solutions approach that of water for sufficiently low BGE concentrations, and the small resulting current produced by ion transport in the channel at such low concentrations can exceed the limit of practical current sensing capabilities due to the inherently low electrical conductance of nanofluidic channels [35–40].

Induced pressure gradients within nanochannels experiencing nonuniform EOF can also pose practical difficulties. In particular, electrokinetic systems with large nonuniform electric fields can lead to structural deformation, channel collapse, cavitation, and delamination of bonded wafers [42,43]. For the current configuration in which  $\zeta_1 < \zeta_2 < 0$ , the higher magnitude of  $\zeta_1$  generally leads to a higher EOF component of the fluid flow in region 1, and by continuity an adverse pressure gradient must be generated in this region to balance the average sum of the pressure-driven flow and electroosmotic flow components in both regions. Therefore, cavitation is unlikely to occur because the positive pressure gradient in region 1 leads to a positive gauge pressure in the middle of the channel. Moreover, the lowest pressure predicted by our simulations was on the order of  $-1 \times 10^{-2}$  bar, well below the critical pressure of  $-16$  bar at which cavitation is theoretically predicted to occur [42]. Structural deformation or wafer debonding could potentially be an issue for more extreme conditions than those we investigate, but the maximum fluid pressure achieved in our simulations is slightly below 3 kPa, several orders of magnitude below the typical bond strength of standard microfabrication techniques [43].

Finally, it should be noted that the current model neglects the presence of  $\text{H}^+$  and  $\text{OH}^-$  ions due to non-neutral solution  $pH$  and dissociation of surface silanol groups at the channel walls. Depending on the solution properties, these effects may also need to be taken into account when calculating the volumetric charge density. Consideration of  $\text{H}^+$  and  $\text{OH}^-$  ions in previous studies [38,39] suggests that there is a limited  $pH$  range over which the concentration of these ions significantly differs from the BGE ion concentrations and can subsequently be neglected. For solutions with sufficiently high or low  $pH$ , the relatively high concentration of  $\text{OH}^-$  or  $\text{H}^+$  ions, respectively, leads to additional charge screening effects which introduce error in the resulting potential and BGE profiles if neglected. By comparing the relative bulk ion concentrations in the reservoirs from electroneutrality conditions, we can expect an estimated error of more than 10% in the spatial charge density if we neglect  $\text{H}^+$  and  $\text{OH}^-$  ions in a KCl solution with a concentration below  $1 \mu\text{M}$ , regardless of solution  $pH$ . Increasing the concentration by an order of magnitude to  $C_{\text{KCl}} = 0.01 \text{ mM}$ , however, leads to a charge density error that is only expected to exceed 10% if the  $pH$  is outside the approximate range of  $6 < pH < 8$  (see the Supplemental Material [34]).

#### IV. CONCLUDING REMARKS

In this work, we demonstrate the use of COMSOL Multiphysics to model the 2D electroosmotic flow of a dilute background electrolyte and the subsequent electrophoretic stacking or focusing of sample ions in a nanofluidic channel with selectively modified surface charge and potential. We first verified our 2D model by comparison with a simplified, approximate 1D area-averaged model for several limiting cases, and then we investigated the possible preconcentration mechanisms within the channel as the wall zeta potential was selectively varied. Our results indicate that the area-averaged electrostatic potential gradient between two regions of nonuniform, overlapped EDLs in a nanochannel generates a midchannel concentration polarization interface which can be used to efficiently focus analyte ions. In addition to this CP-based focusing mechanism, FASS-like stacking and focusing can also be achieved for charged samples of certain mobility in cases with nonoverlapped EDLs. It is therefore theoretically possible to perform stationary field-amplified sample preconcentration in nanochannels without introducing multiple electrolyte solutions, but by simply inducing electric field gradients through the tailoring of wall surface potential uniformity via embedded electrodes. We show that the dominant midchannel CP focusing effect only occurs in channels with sufficiently large step changes in zeta potential and in which the EDL thickness is comparable to or exceeds the channel height. Our results suggest that sample enhancement ratios exceeding  $10^5$  are potentially achievable, notably higher than those typically limited by sample dispersion in conventional FASS with high plug-to-background conductivity ratios [8–11]. Moreover, the enhancement ratios predicted by our simulations are within an order of magnitude of the million-fold preconcentration levels that are possible using more refined nanoscale methods such as standard CP-based techniques and isotachopheresis [13,18]. The efficacy and flexibility of this proposed technique leads us to conclude that there is potential for further improvement and optimization of various analyte preconcentration processes by embedding gate electrodes to manipulate local ion transport within nanofluidic channels.

#### ACKNOWLEDGEMENT

We greatly acknowledge our funding sources, the Institute for Collaborative Biotechnologies through Grant W911NF-09-001 from the U.S. Army Research Office and Grant DAAD19-03-D-0004 from the U.S. Army Research Office.

- 
- [1] T. C. Kuo, D. M. Cannon, Y. Chen, J. J. Tulock, M. A. Shannon, J. V. Sweedler, and P. W. Bohn, Gateable nanofluidic interconnects for multilayered microfluidic separation systems, *Anal. Chem.* **75**, 1861 (2003).
  - [2] M. Napoli, J. C. T. Eijkel, and S. Pennathur, Nanofluidic technology for biomolecule applications: A critical review, *Lab Chip* **10**, 957 (2010).
  - [3] Y. Ai, J. Liu, B. Zhang, and S. Qian, Field effect regulation of DNA translocation through a nanopore, *Anal. Chem.* **82**, 8217 (2010).
  - [4] W. Sparreboom, A. van den Berg, and J. C. T. Eijkel, Principles and applications of nanofluidic transport, *Nature Nanotechnol.* **4**, 713 (2009).
  - [5] Y. Liu and L. Yobas, Slowing DNA translocation in a nanofluidic field-effect transistor, *ACS Nano* **10**, 3985 (2016).
  - [6] D. Stein, Z. Deurvorst, F. H. J. van der Heyden, W. J. A. Koopmans, A. Gabel, and C. Dekker, Electrokinetic concentration of DNA polymers in nanofluidic channels, *Nano Lett.* **10**, 765 (2010).
  - [7] J. Fu, R. B. Schoch, A. L. Stevens, S. R. Tannenbaum, and J. Han, A patterned anisotropic nanofluidic sieving structure for continuous-flow separation of DNA and proteins, *Nature Nanotechnol.* **2**, 121 (2007).
  - [8] D. S. Burgi and R. L. Chien, Optimization in sample stacking for high-performance capillary electrophoresis, *Anal. Chem.* **63**, 2042 (1991).

- [9] R. Bharadwaj and J. G. Santiago, Dynamics of field-amplified sample stacking, *J. Fluid. Mech.* **543**, 57 (2005).
- [10] J. M. Susterich, B. D. Storey, and S. Pennathur, Field-amplified sample stacking and focusing in nanofluidic channels, *Phys. Fluids* **22**, 112003 (2010).
- [11] B. Jung, R. Bharadwaj, and J. G. Santiago, Thousandfold signal increase using field-amplified sample stacking for on-chip electrophoresis, *Electrophoresis* **24**, 3476 (2003).
- [12] Q. Pu, J. Yun, H. Temkin, and S. Liu, Ion-enrichment and ion-depletion effect of nanochannel structures, *Nano Lett.* **4**, 1099 (2004).
- [13] Y. C. Wang, A. L. Stevens, and J. Han, Million-fold preconcentration of proteins and peptides by nanofluidic filter, *Anal. Chem.* **77**, 4293 (2005).
- [14] A. Mani, T. A. Zangle, and J. G. Santiago, On the propagation of concentration polarization from microchannel-nanochannel interfaces Part I: Analytical model and characteristic analysis, *Langmuir* **25**, 3898 (2009).
- [15] T. A. Zangle, A. Mani, and J. G. Santiago, Theory and experiments of concentration polarization and ion focusing at microchannel and nanochannel interfaces, *Chem. Soc. Rev.* **39**, 1014 (2010).
- [16] A. Plecis, C. Nanteuil, A. Haghiri-Gosnet, and Y. Chen, Electropreconcentration with charge-selective nanochannels, *Anal. Chem.* **80**, 9542 (2008).
- [17] S. J. Kim, Y. Song, and J. Han, Nanofluidic concentration devices for biomolecules utilizing ion concentration polarization: Theory, fabrication, and applications, *Chem. Soc. Rev.* **39**, 912 (2010).
- [18] B. Jung, R. Bharadwaj, and J. G. Santiago, On-chip millionfold sample stacking using transient isotachophoresis, *Anal. Chem.* **78**, 2319 (2006).
- [19] W. L. Hsu, D. W. Inglis, M. A. Startsev, E. M. Goldys, M. R. Davidson, and D. J. Harvie, Isoelectric focusing in a silica nanofluidic channel: Effects of electromigration and electroosmosis, *Anal. Chem.* **86**, 8711 (2014).
- [20] W. L. Hsu, D. J. Harvie, M. R. Davidson, H. Jeong, E. M. Goldys, and D. W. Inglis, Concentration gradient focusing and separation in a silica nanofluidic channel with a non-uniform electroosmotic flow, *Lab Chip* **14**, 3539 (2014).
- [21] R. B. M. Schasfoort, S. Schlautmann, J. Hendrikse, and A. van den Berg, Field-effect flow control for microfabricated fluidic networks, *Science* **286**, 942 (1999).
- [22] A. E. Herr, J. I. Molho, J. G. Santiago, M. G. Mungal, and T. W. Kenny, Electroosmotic capillary flow with nonuniform zeta potential, *Anal. Chem.* **72**, 1053 (2000).
- [23] L. M. Fu, J. Y. Lin, and R. J. Yang, Analysis of electroosmotic flow with step change in zeta potential, *J. Colloid Interface Sci.* **258**, 266 (2003).
- [24] G. Pardon and W. van der Wijngaart, Modeling and simulation of electrostatically gated nanochannels, *Adv. Colloid Interface Sci.* **199-200**, 78 (2013).
- [25] R. Karnik, R. Fan, M. Yue, D. Li, P. Yang, and A. Majumdar, Electrostatic control of ions and molecules in nanofluidic transistors, *Nano Lett.* **5**, 943 (2005).
- [26] H. Daiguji, Y. Oka, and K. Shirono, Nanofluidic diode and bipolar transistor, *Nano Lett.* **5**, 2274 (2005).
- [27] T. Maleki, S. Mohammadi, and B. Ziaie, A nanofluidic channel with embedded transverse electrodes, *Nanotechnology* **20**, 105302 (2009).
- [28] Y. J. Oh, A. L. Garcia, D. N. Petsev, G. P. Lopez, S. R. J. Brueck, C. F. Ivory, and S. M. Han, Effect of wall-molecule interactions on electrokinetic transport of charged molecules in nanofluidic channels during FET flow control, *Lab Chip* **9**, 1601 (2009).
- [29] H. Daiguji, Ion transport in nanofluidic channels, *Chem. Soc. Rev.* **39**, 901 (2010).
- [30] Z. Jiang and D. Stein, Charge regulation in nanopore ionic field-effect transistors, *Phys. Rev. E* **83**, 031203 (2011).
- [31] X. Jin and N. R. Aluru, Gated transport in nanofluidic devices, *Microfluid Nanofluid* **11**, 297 (2011).
- [32] W. Guan, S. X. Li, and M. A. Reed, Voltage gated ion and molecule transport in engineered nanochannels: Theory, fabrication, and applications, *Nanotechnology* **25**, 122001 (2014).
- [33] S. H. Lee, H. Lee, T. Jin, S. Park, B. J. Yoon, G. Y. Sung, K. B. Kim, and S. J. Kim, Sub-10 nm transparent all-around-gated ambipolar ionic field effect transistor, *Nanoscale* **7**, 936 (2015).

- [34] See Supplemental Material at <http://link.aps.org/supplemental/10.1103/PhysRevFluids.2.124203> for simulation parameters, 1D area-averaged model, and supplemental figures.
- [35] D. Stein, M. Kruithof, and C. Dekker, Surface-Charge-Governed ion Transport in Nanofluidic Channels, *Phys. Rev. Lett.* **93**, 035901 (2004).
- [36] F. Baldessari and J. G. Santiago, Corrigendum to “Electrokinetics in nanochannels. Part I. Electric double layer overlap and channel-to-well equilibrium” [*J. Colloid Interface Sci.* **325**, 526 (2008)], *J. Colloid Interface Sci.* **331**, 549 (2009).
- [37] K. L. Jensen, J. T. Kristensen, A. M. Crumrine, M. B. Andersen, H. Bruus, and S. Pennathur, Hydronium-dominated ion transport in carbon-dioxide-saturated electrolytes at low salt concentration in nanochannels, *Phys Rev. E* **83**, 056307 (2011).
- [38] L. H. Yeh, Y. Ma, S. Xue, and S. Qian, Gate manipulation of ionic conductance in a nanochannel with overlapped electric double layers, *Sensors Actuators B* **215**, 266 (2015).
- [39] C. Hughes, L. H. Yeh, and S. Qian, Field effect modulation of surface charge property and electroosmotic flow in a nanochannel: Stern layer effect, *J. Phys. Chem. C* **117**, 9322 (2013).
- [40] C. McCallum and S. Pennathur, Accounting for electric double layer and pressure gradient-induced dispersion effects in microfluidic current monitoring, *Microfluid Nanofluid* **20**, 13 (2016).
- [41] S. Behrens and D. G. Grier, The charge of glass and silica surfaces, *J. Chem. Phys.* **115**, 6716 (2001).
- [42] D. S. van Schoot, K. G. H. Janssen, N. R. Tas, T. Hankemeier, and J. C. T. Eijkel, *Electrocavitation in Nanochannels*, edited by L. Mercury, N. Tas, and M. Zilberbrand, in *Transport and Reactivity of Solutions in Confined Hydrosystems*, NATO Science for Peace and Security Series C: Environmental Security (Springer, Dordrecht, 2014).
- [43] J. M. de Rutte, K. G. H. Janssen, N. R. Tas, J. C. T. Eijkel, and S. Pennathur, Numerical investigation of micro- and nanochannel deformation due to discontinuous electroosmotic flow, *Microfluidics Nanofluidics* **20**, 150 (2016)